Mathematical Biosciences and Engineering

http://www.aimspress.com/journal/mbe

MBE, 20(1): 1274–1296.
DOI: 10.3934/mbe.2023058
Received: 24 August 2022
Revised: 03 October 2022
Accepted: 10 October 2022
Published: 27 October 2022

Research article

A transient biological fouling model for constant flux microfiltration

Vincenzo Luongo[1,*], Maria Rosaria Mattei[1], Luigi Frunzo[1], Berardino D'Acunto[1], Kunal Gupta[2], Shankararaman Chellam[2,3] and Nick Cogan[4]

[1] Department of Mathematics and Applications "Renato Caccioppoli", University of Naples Federico II, via Cintia, Monte S. Angelo, Naples, I-80126, Italy

[2] Department of Civil & Environmental Engineering, Texas A & M University, College Station, TX 77843, USA

[3] Department of Chemical Engineering, Texas A & M University, College Station, TX 77843, USA

[4] Department of Mathematics, Florida State University, 208 Love Building, Tallahassee, FL 32306-4510, USA

* **Correspondence:** Email: vincenzo.luongo@unina.it.

Abstract: Microfiltration is a widely used engineering technology for fresh water production and water treatment. The major concern in many applications is the formation of a biological fouling layer leading to increased hydraulic resistance and flux decline during membrane operations. The growth of bacteria constituting such a biological layer implicates the formation of a multispecies biofilm and the consequent increase of operational costs for reactor management and cleaning procedures. To predict the biofouling evolution, a mono-dimensional continuous free boundary model describing biofilm dynamics and EPS production in different operational phases of microfiltration systems has been well studied. The biofouling growth is governed by a system of hyperbolic PDEs. Substrate dynamics are modeled through parabolic equations accounting for diffusive and advective fluxes generated during the filtration process. The free boundary evolution depends on both microbial growth and detachment processes. What is not addressed is the interplay between biofilm dynamics, filtration, and water recovery. In this study, filtration and biofilm growth modeling principles have been coupled for the definition of an original mathematical model able to reproduce biofouling evolution in membrane systems. The model has been solved numerically to simulate biologically relevant conditions, and to investigate the hydraulic behavior of the membrane. It has been calibrated and validated using lab-scale data. Numerical results accurately predicted the pressure drop occurring in the microfiltration system. A calibrated model can give information for optimization protocols as well as fouling prevention strategies.

Keywords: microfiltration; biofouling; biofilms; free boundary value problem; numerical simulations

1. Introduction

Membrane technology has been largely used as one of the most promising engineering strategies for both wastewater treatment and fresh water production [1]. Due to the increasing water demands for human, industrial, and agricultural use, many applications to provide clean water have been developed, primarily differentiated by membrane porosity, i.e., ultrafiltration, microfiltration, nanofiltration and reverse osmosis. The major concern in all these applications is the formation of a colloidal inorganic (e.g., scale) and/or biological (e.g., bacteria, organic particle flocs, bio-polymers) fouling layer [2]. The latter is strongly influenced by the specific context as it depends on membrane characteristics and water quality. The accumulation of particles and the formation of a cake layer on membrane surfaces lead to increasing hydraulic resistance and productivity decline [3]. This represents a significant operational cost in terms of energy and chemicals for cleaning procedures [4].

Membrane performance is highly dependent on the characteristics of the treated water, e.g., macro/micro nutrient content, total and suspended solid content, and on the specific environment where the filtration process occurs. In the case of membrane bio-reactors (MBR), polymeric membranes for solid/liquid separation are used in bio-reactors where specific biological processes are catalyzed allowing for high quality effluents, low sludge production, and improved nutrient removal [5]. For instance, organic carbon removal and nitrification process, operated by heterotrophic and autotrophic species, respectively, lead to the growth and accumulation of bacteria, which aggregate in active sludge flocs in aerated conditions and are able to ensure high quality of wastewater treatment plants effluents [6–8]. Clearly, the direct contact of the membrane surface and bacterial flocs and microorganisms stimulates the formation of a mainly biological fouling layer constituting a multispecies biofilm.

Submerged membranes are bound to be colonized by bacteria [9]; they represent a perfect environment for biofilm growth and evolution. Initially, biofilms have a beneficial effect due to their ability to remove biodegradable pollutants [10]. Afterwords, they are responsible for an unacceptable decline of membrane performance, reduced water quality, and biodeterioration of membranes components [9, 11]. Over the last decades, mathematical modeling of membrane filtration systems have been largely studied using classical blocking laws [12–14]. These are classified by the size of particulate foulants approaching the membrane and the size of pores constituting the filtration membrane. Two different approaches have been used for blocking law formulation: the constant flux J approach, where increasing hydraulic resistance leads to increasing pressure drop $\Delta P(t)$; the constant pressure approach, where J is a function of time and ΔP is a constant. These approaches reflect the conventional operation strategies usually adopted in membrane reactors. Despite the usefulness and accuracy of such models in diagnosing the hydraulic behavior both in forward operation and after backwashing, these models lack biological and kinetic description of fouling formation and development, as well as predictive ability.

Due to recent advances in mathematical modeling of multispecies biofilms and recent improvements in microscopy and imaging techniques [15–19], many researchers have begun to focus on the structural organization and rheological response of biofilms growing on membrane systems [9, 20]. Vrouwenvelder et al. [21] assessed that the extracellular polymeric substances (EPS) constituting a biofilm exclusively determine its hydraulic resistance. In addition, the authors highlighted the negligible effect of bacterial cells embedded in the biofilm matrix. They proposed a 3-D mathematical formulation to predict the increase of hydraulic resistance during the permeation of water in a rectangular domain.

Tierra et al. [22] introduced a phase-field multicomponent model to investigate the effect of EPS viscosity and elasticity on biofilm deformation. The authors were able to numerically reproduce the effect of the shear flow on the detachment rate by using flow cell experiments to determine the mechanical characteristics of the investigated biofilm. Recently, Li et al. [23] proposed a phase-field continuum model coupled with the Oldroyd-B constitutive equation to simulate biofilm deformation under stress conditions. The model predicted with high accuracy the viscoelastic deformation of different mature biofilms constituting a useful tool for engineering biofilm systems control. However, all these models completely neglect the biological dynamics, the contribution of biofilm growth on fouling, and the related reduction in filtration capacity occurring in membrane systems.

Other authors explored the mathematical modeling of membrane reactors exclusively focusing on the quality of effluents, or on the hydraulic response of biofilms under different stress conditions [24–26]. More sophisticated multidimensional models have been also proposed to describe the non-uniform development of particulate fouling layers and their heterogeneous morphology in high pressure cross-flow filtration membranes [27,28]. Several of the authors here have studied the fouling and regeneration process, focusing on developing models that are amendable to optimal control analysis and extensions to more realistic models [29, 30].

To the best of our knowledge, mathematical models accounting for both detailed biofilm growth dynamics and EPS production during the operational phases of membrane reactors have not yet been developed. Therefore, this work connects insights related to membrane filtration, and growth and development of multispecies biofilms occurring in submerged filters. It aims at the development of a mathematical tool able to describe the filtration and backwashing effect on biofilm systems and the biofouling kinetics effect on the hydraulic behavior in microfiltration membrane systems. It represents a first step in the development of more complex mathematical models able to assist membrane facilities in designing and operational procedures.

The work includes observations of membrane/biofilm interaction, such as monodimensional spatial distribution of biofilm components, and substrate dynamics, and physical effects of backwashing on biofilm growth. The model was calibrated and validated by using experimental data obtained with a lab scale membrane system under different operating conditions (filtration time of 20 and 40 *min*). Numerical simulations remarked on the consistency of the model and showed the effect of substrate diffusion/convection and biofilm detachment during forward and backwashing operations.

2. Filtration principles and biofilm growth

The microfiltration mathematical problem is here presented as a multi-scale model, where the pressure drop during water filtration (macroscale) is directly influenced by biofilm growth and development on the dead-end membrane surface (microscale). Simultaneously, the effect of backwashing on biofilm dynamics, which affects the detachment rate and the free boundary problem describing biofilm thickness evolution, has been included in the present formulation.

A schematic of the operational conditions of the filtration system during the filtration and regeneration phases is shown in Figure 1. During forward filtration, the wastewater is forced to pass through the membrane with consequent particles accumulation and biofilm growth stimulation. In the backwashing or regeneration regimen, clean water is added to the system from the membrane surface to the bulk liquid as this practice partially removes previously formed cake layer including the biofilm.

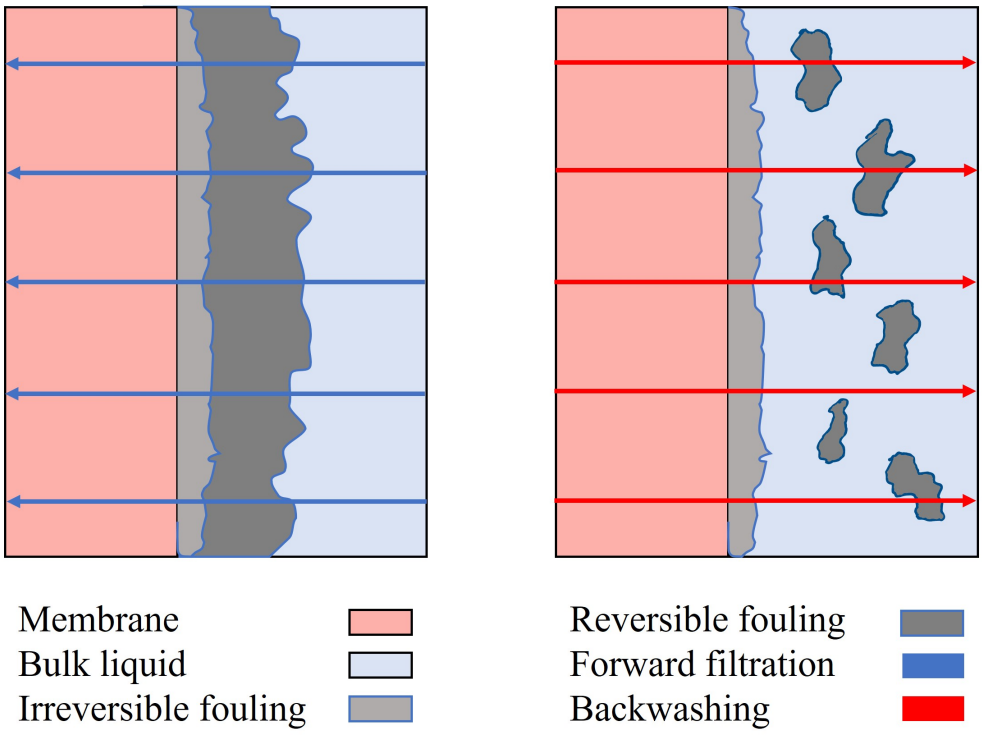

Figure 1. Schematic representation of MBR operational conditions: forward filtration (left) and backwashing operations (right).

Assuming constant flux J operation during water filtration, the pressure drop $\Delta P(t)$ is defined by a Darcy's law based formulation as:

$$\Delta P(t) = J\mu\left(R_m + R_B(t)\right), \tag{2.1}$$

where μ is the absolute viscosity of water, R_m is the hydraulic resistance of the clean membrane, and R_B is the hydraulic resistance due to the presence of the biofilm layer. The constant flux assumption is motivated by engineering applications of the system. In Eq (2.1), the hydraulic resistance of the biofilm layer R_B is a function of the mass of foulants, i.e., biofilm components, accumulating on the membrane surface and constituting the biofouling cake.

A well-studied model of the dynamics of a one-dimensional biofilm is based on the Wanner-Gujer model [31–34]. As this model is used as the core fouling process model in the current study, a brief overview of the notation and variables is given. The multispecies biofilm dynamics have been modeled as an essentially hyperbolic free boundary problem. The evolution of the biofilm thickness L, which represents the free boundary [35], is governed by the growth of biofilm components $X_i(z,t)$, $i = 1, ..., n$, and the availability of substrates $S_j(z,t)$, $j = 1, ..., m$ within the biofilm. Note that X_i and S_j are both concentrations $[mgL^{-1}]$, and each of the i^{th} biofilm component can be expressed in terms of biofilm volume fraction f_i as $X_i = \rho_i f_i$, $i = 1, ..., n$, where ρ_i is the density in $[mgL^{-1}]$ of the i^{th} biofilm component [34, 36, 37]. These components are generally named biomasses and can be categorized

as microbial species, which evolve over time due to their metabolic activities, and other biologically produced components, such as inert materials or extracellular polymeric substances (EPS), which are generated by living cells and accumulate in the biofilm matrix. For instance, the EPS fraction confers to the biofilm structure specific functions including the enhancement of the mechanical resistance [38].

The dynamics of biofilm components are derived from local mass balance considerations, and the hyperbolic system of Equations is described as:

$$\frac{\partial X_i}{\partial t} + \frac{\partial}{\partial z}(uX_i) = \rho_i r_{M,i}(z,t,\mathbf{X},\mathbf{S}), \;\; i = 1,...,n, \;\; 0 \le z \le L(t), \; t > 0, \tag{2.2}$$

where $u(z,t)$ is the velocity of microbial mass displacement with respect to the membrane surface, $r_{M,i}(z,t,\mathbf{X},\mathbf{S})$ is the biomass growth rate, $\mathbf{X} = (X_i,...,X_n)$, and $\mathbf{S} = (S_j,...,S_m)$. The metabolic reactions operated by bacterial species are able to generate an advective flux described as a mass displacement, and dominated by microbial growth, decay reactions, and EPS production. The velocity of microbial mass displacement $u(z,t)$ is obtained by summing Eq (2.2) over i,

$$\frac{\partial u}{\partial z} = \sum_{i=1}^{n} r_{M,i}(z,t,\mathbf{X},\mathbf{S}), \;\; 0 < z \le L(t), \; t \ge 0, \tag{2.3}$$

and considering the volume fraction constrain $\sum_{i=1}^{n} f_i = 1$. The multispecies biofilm growth model is completed by using an ordinary differential equation describing the evolution of the biofilm thickness $L(t)$ as a free boundary layer. The variation of biofilm thickness over time is described as:

$$\dot{L}(t) = u(L(t),t) - \sigma_d(L(t)), \;\; t > 0, \tag{2.4}$$

which is a function of both the microbial mass displacement velocity and the detachment flux $\sigma_d(L(t))$. The latter is directly connected to membrane operation, as it accounts for the sloughing phenomenon occurring during backwashing operations.

To connect the biofilm dynamics with the filtration process, it is necessary to specify how the water flow direction (e.g., filtration or backwashing/regeneration) affects the biofilm dynamics and also how the biofilm dynamics affect the filtration process. The former is incorporated in two ways. First, the filtration direction affects the attachment/detachment processes. According to previous studies [34, 39, 40], the proposed sloughing rate assumes that the loss of biofilm mass is proportional to the biofilm thickness. In addition, it can take into account that the EPS volume fraction is more resistant than all the other biofilm component to the hydraulic stress [21], and it negatively influences the efficiency of the cleaning procedure applied with the backwashing phase. The formulation of the detachment rate proposed in the present study is described as:

$$\sigma_d(L(t)) = \lambda L^2 + K\left(\frac{|J| + J}{2}\right)\left(1 - \hat{f}_{EPS}\right)(L - L_{lim}), \tag{2.5}$$

where, J is the constant flux applied for the membrane filtration and the backwashing procedure, $\hat{f}_{EPS}$ is the average EPS volume fraction along the biofilm thickness, K is the sloughing constant $[m^{-1}]$, and L_{lim} is an irreversible fouling layer that is not removed by backwashing procedures. Note that the second term on the right hand side of Eq (2.5) is equal to zero when the filtration flux J is non-positive, and this condition occurs when the water is filtered throughout the membrane surface or it is not filtered

for MBR maintenance procedures. Thus the second term links the membrane operation and the foulant layer structure to the physical cleaning provided by backwashing. The second effect of the filtration direction on the biofilm dynamics is through the substrate distribution. In particular, the bacterial growth is catalyzed by the presence of m different substrates in the treated water, which are able to influence the metabolic activity of the considered microbial species constituting the biofilm. The evolution of substrates over time and space has been modeled as a system of nonlinear convection−diffusion−reaction equations:

$$\frac{\partial S_j}{\partial t} - \frac{\partial}{\partial z}\left(D_{S,j}\frac{\partial S_j}{\partial z}\right) + v\frac{\partial S_j}{\partial z} = r_{S,j}(z,t,\mathbf{X},\mathbf{S}), \quad j = 1,...,m, \quad 0 < z < L(t), \; t > 0, \tag{2.6}$$

where $D_{S,j}$ is the diffusivity coefficient, v is the filtration velocity, $S_j(z,t)$ represents the concentration of the substrate S_j, $j = 1,...,m$, and $r_{S,j}(z,t,\mathbf{X},\mathbf{S})$ is the conversion rate of each substrate j. Due to the presence of the membrane, the filtration velocity v is proportional to the constant filtration flux J in both filtration and backwashing/regeneration regimes. Denoting with S the filtration surface, which is the area where the water is forced to pass trough the membrane, it is possible to assume that:

$$J = \frac{v}{S}. \tag{2.7}$$

Assuming $S = 1$, from Eq (2.7) it is evident that J and v have the same negative or positive value during the filtration or backwashing/regeneration regimes, respectively. This aspect is crucial to explain the effect of the filtration direction on substrate concentrations within the biofilm during different membrane operations: the dissolved substrates diffuse within the biofilm and contextually are transported by the liquid flow, as highlighted in Section 5 with a numerical example.

Just as the filtration regime affects the biofilm dynamics, the presence of the biofilm directly affects the filtration. Using the detailed microscale model, it is possible to capture the effects of the biofilm structure on the fouling process rather than relegating the process to a bulk, empirical model. Despite many simplistic membrane models describing the filtration mechanism as a process merely affected by particle sizes and membrane characteristics (e.g., blocking laws), the definition of R_B in Eq (2.1) allows to elucidate the relation between the biofouling kinetic evolution and the hydraulic (Darcy-based) resistance in in-series filtration processes. This aspect is crucial as in both real scale and lab scale experiments the hydraulic resistance of membrane reactors is strongly influenced by biological dynamics and by bacteria attached on the membrane surface. According to experimental evidences [21], various components constituting a biofouling layer can differently affect the pressure drop during microfiltration. Moreover, a specific hydraulic resistance α_i, $i = 1,...,n$ has been assumed for each biofilm component, so that the pressure drop during constant flow microfiltration can be assumed as a proportional function of the mass of each specific biofilm component constituting the biofouling layer. Equation (2.1) can be rewritten in the form:

$$\Delta P(t) = J\mu\left(R_m + \sum_{i=1}^{n}\alpha_{0,i}\int_0^{L(t)}\frac{f_i\rho_i}{L_0}z\,dz\right), \tag{2.8}$$

where $\alpha_{0,i}$, f_i, and ρ_i are the specific resistance, the volume fraction, and the density of each i^{th} biofilm component, respectively. Note that, assuming a mono-species biofilm ($f_1 = 1$), Eq (2.8) leads to

$$\Delta P(t) = \mu \left(R_m + \frac{\alpha_1 \rho_1 L^2(t)}{2L_0} \right) J, \tag{2.9}$$

where the relation between the pressure drop $\Delta P(t)$ and the biofilm thickness $L(t)$ is highlighted. Note that this is a novel connection between the detailed resistance, calculated based on the dynamics of the fouling layer and the macroscopic fouling laws.

3. Initial and boundary conditions

The forward and backwashing problem is treated by setting different initial-boundary conditions related to the systems of nonlinear partial differential Eqs (2.2)–(2.4) and (2.6). For Eq (2.2), the initial conditions

$$X_i(z, 0) = X_{i0}(z), \quad i = 1, ..., n, \quad 0 \le z \le L_0, \tag{3.1}$$

have been prescribed, where $X_{i0}(z)$ are general positive functions associated to the different components constituting the initial biofilm structure. A no flux condition has been set on the substratum in Eq (2.3) and the initial value for $L(t)$ has been defined in Eq (2.4) as:

$$u(0, t) = 0, \quad t \ge 0, \quad L(0) = L_0, \tag{3.2}$$

where L_0 is a positive constant. The initial substrate concentration profiles $S_j(z, 0)$ are directly affected from the substrate concentrations in the secondary treated wastewater, and are defined as

$$S_j(z, 0) = S_{j0}(z), \quad j = 1, ..., m, \quad 0 \le z \le L_0, \tag{3.3}$$

where $S_{j0}(z)$ are assigned positive functions. The forward filtration problem is solved by adopting the boundary conditions for $J < 0$

$$\frac{\partial S_j}{\partial z}(0, t) = 0, \quad \frac{\partial S_j}{\partial z}(L, t) = \frac{v}{D_j} \left(S_{jL}(t) - S_j(L, t) \right), \quad j = 1, ..., m, \quad t > 0, \tag{3.4}$$

where the functions $S_{jL}(t)$ are related to the substrate concentration in the wastewater. The diffusive flux at $z = 0$ has been set to zero as the concentration value of substrates in the first section of the biofilm layer is equivalent to the concentration in the permeate flux (treated water). Moreover, the variation of substrates at $z = L(t)$ is described as a filtration flux, which is directly influenced by the concentration of substrates in the wastewater $S_{jL}(t)$, and by the filtration flux J. The forward filtration phase is followed by a zero flux phase $J = 0$ required for membrane maintenance. In this phase, the boundary conditions for Eq (2.6) assume the following form

$$\frac{\partial S_j}{\partial z}(0, t) = 0, \quad \frac{\partial S_j}{\partial z}(L, t) = 0, \quad j = 1, ..., m, \ t > 0, \tag{3.5}$$

as the advective flux zero and the water is not fed to the MBR system from both the membrane sides. After a zero flux phase, the backwashing procedure begins with reversing the water flow $J > 0$, and clean water enters in the system from the initial biofilm layer ($z = 0$) to the moving boundary ($z = L(t)$).

To solve the system of Eq (2.6), Robin and Neumann boundary conditions have been prescribed at $z = 0$ and $z = L$, respectively,

$$\frac{\partial S_j}{\partial z}(0,t) = \frac{v}{D_j} S_j(0,t), \quad \frac{\partial S_j}{\partial z}(L,t) = 0, \quad j = 1, ..., m, \ t > 0. \tag{3.6}$$

Equation (3.6) describes the substrate fluxes applied on the biofouling layer during the cleaning operation procedures. It is a common practice to use just water during backwashing to clean the membrane and mitigate the biofouling formation. For this reason, just an advective flux was adopted for the substrate concentrations at $z = 0$. On the other hand, at $z = L$ a Neumann condition was set as it was assumed that the effect of substrates concentration in the bulk liquid $S_{jL}(t)$ is negligible with respect to the filtration flux J.

4. Model application

The mathematical model was specified to simulate the heterotrophic-autotrophic competition for oxygen usually occurring in wastewater treatment. In this context, it is possible to remove nutrients from wastewater by catalyzing the microbial metabolism of these species, and providing oxygen to the biological units of the wastewater treatment plant. This strategy leads to the effective decrease of nutrient concentrations in the water and provides a clean effluent with enhanced water quality. For the specific application, a constant density $\rho = \rho_i, \ i = 1, ..., n$ has been assumed for all the biofilm components, and 4 different components have been considered $n = 4$. The modeled microbial species, such as autotrophic X_1 and heterotrophic bacteria X_2, are able to produce two more biofilm components, i.e., inert material X_3 and EPS X_4, due to their growth and evolution driven by ammonium nitrogen and organic carbon uptake, respectively [7,38]. Indeed, the bacterial growth is catalyzed by the uptake of 3 different substrates, $m = 3$, such as ammonium nitrogen S_1, organic carbon S_2, and dissolved oxygen S_3. The latter is required for both organic carbon removal and nitrification process, operated by the heterotrophic and autotrophic species, respectively.

The kinetic growth rates $r_{Mi}(z, t, \mathbf{X}, \mathbf{S})$ for the biofilm components X_1, X_2, X_3, and X_4 are expressed as Monod-like kinetics and the growth and evolution of each component is dominated by the presence and availability of substrates in time and space. Moreover, they account for different biological mechanisms, such as endogenous respiration, EPS production, decay-inactivation, and biodegradability of microbial components, which usually are included in multispecies biofilm modeling. These lead to non-linear multiparameter expressions describing the dynamics of each biofilm component due to substrates utilization and metabolites production during biofilm evolution. For the bacterial components X_1 and X_2,

$$r_{M,1} = \left((1 - k_1) K_{\max,1} \frac{S_2}{K_{1,2} + S_2} \frac{S_3}{K_{1,3} + S_3} - b_1 F_1 \frac{S_3}{K_{1,3} + S_3} - (1 - F_1) c_1 \right) X_1, \tag{4.1}$$

$$r_{M,2} = \left((1 - k_2) K_{\max,2} \frac{S_1}{K_{2,1} + S_1} \frac{S_3}{K_{2,3} + S_3} - b_2 F_2 \frac{S_3}{K_{2,3} + S_3} - (1 - F_2) c_2 \right) X_2, \tag{4.2}$$

where $K_{\max,i}$ denotes the maximum net growth rate for biomass i, k_i is the coefficient associated to EPS formation, $K_{i,j}$ represents the affinity constant of substrate j for biomass i, b_i denotes the endogenous rate for biomass i, c_i is the decay−inactivation rate for biomass i, and F_i represents the biodegradable

fraction of biomass i. The latter represents a fraction of the microbial component that is converted in composite particulate material due to metabolic reactions. It allows the production in the biofilm matrix of an inert component X_3 whose growth rate is expressed as

$$r_{M,3} = (1 - F_1)c_1X_1 + (1 - F_2)c_2X_2. \tag{4.3}$$

Similarly, the accumulation of the EPS component X_4 within the biofilm matrix is due to bacteria activities during their evolution. The terms $(1 - k_i)$ in Eqs (4.1) and (4.2) indicate that a fraction of available substrates are used by X_1 and X_2 microbial species for EPS formation during the metabolic reactions for biomass production. Moreover, the growth rate for the EPS component X_4 is defined as

$$r_{M,4} = k_1K_{\max,1}\frac{S_2}{K_{1,2} + S_2}\frac{S_3}{K_{1,3} + S_3}X_1 + k_2K_{\max,2}\frac{S_1}{K_{2,1} + S_1}\frac{S_3}{K_{2,3} + S_3}X_2. \tag{4.4}$$

The conversion rates $r_{S,j}(z, t, \mathbf{X}, \mathbf{S})$, $j = 1, 2, 3$, related to substrates utilization for metabolic activities are described as Monod-like kinetics, which define the consumption of ammonia S_1, organic carbon S_2 and oxygen S_3 by biofilm components. These are described as follows:

$$r_{S,1} = -\frac{1}{Y_2}\left((1 - k_2)K_{\max,2}\frac{S_1}{K_{2,1} + S_1}\frac{S_3}{K_{2,3} + S_3}\right)X_2, \tag{4.5}$$

$$r_{S,2} = -\frac{1}{Y_1}\left((1 - k_1)K_{\max,1}\frac{S_2}{K_{1,2} + S_2}\frac{S_3}{K_{1,3} + S_3}\right)X_1, \tag{4.6}$$

$$\begin{aligned} r_{S,3} = &-\frac{(1 - Y_1)}{Y_1}\left((1 - k_1)K_{\max,1}\frac{S_2}{K_{1,2} + S_2}\frac{S_3}{K_{1,3} + S_3}\right)X_1 \\ &-\frac{(1 - Y_2)}{Y_2}\left((1 - k_2)K_{\max,2}\frac{S_1}{K_{2,1} + S_1}\frac{S_3}{K_{2,3} + S_3}\right)X_2 \\ &-b_{m,1}F_1\frac{S_3}{K_{1,3} + S_3}X_1 - b_{m,2}F_2\frac{S_3}{K_{2,3} + S_3}X_2, \end{aligned} \tag{4.7}$$

where Y_i denotes the yield for each biomass i.

5. Experimental set up and and numerical simulations

The proposed mathematical model was used to reproduce lab scale experiments performed with 4 polyvinylidene fluoride (PVDF) hollow fiber membranes operated at a constant flux of 60 $Lm^{-2}h^{-1}$ during forward microfiltration. The total surface of the membrane modules was 30 cm^2 and a secondary treated wastewater was fed to the system with a dissolved organic carbon (DOC) content around 6.2 ± 0.12 mgL^{-1}, corresponding to a chemical oxygen demand (COD) content of about 25 mgL^{-1} [41]. Different timing for forward filtration were used in two experimental sets, where the membranes were backwashed at 20 or 40 minutes intervals. Moreover, the same backwashing procedure was adopted in both the experimental sets. It consists in a 90 s flushing phase to remove the permeate and fill the tubes with ultra-pure water, followed by a 60 s backwashing step with ultra-pure water at the same working flux J. In addition, a 30 s gravity drain was applied, in order to completely empty the membrane modules, and a 100 s forward flushing phase was applied to fill the membrane modules with the feed

wastewater, prior to start with the further filtration cycle. In all experimental cases, the total specific filtered volume was 720 Lm^{-2}.

Virgin and fouled membranes were stained with two fluorescent dyes simultaneously: 4',6-diamidino-2-phenylindole dihydrochloride (DAPI), and 5-cyano-2,3-ditolyl tetrazolium chloride (CTC) (Biotium, CA) to observe total and live bacterial cells under the microscope, respectively [42]. DAPI fluoresces upon binding to DNA [42], whereas CTC dye is reduced and fluoresces when there is an electron transport, implying actively respiring bacteria [43]. Stained samples were imaged using an Olympus BX53 microscope. The backwashing procedure was modeled with a zero flux phase of 90 s followed by a reversed flux phase of 60 s. The biofilm-membrane model was able to reproduce the cleaning procedure with a zero flux $J = 0$ and a reversed flux $J = 60\ Lm^{-2}h^{-1}$ phase prior to start a new forward filtration $J = -60\ Lm^{-2}h^{-1}$ cycle.

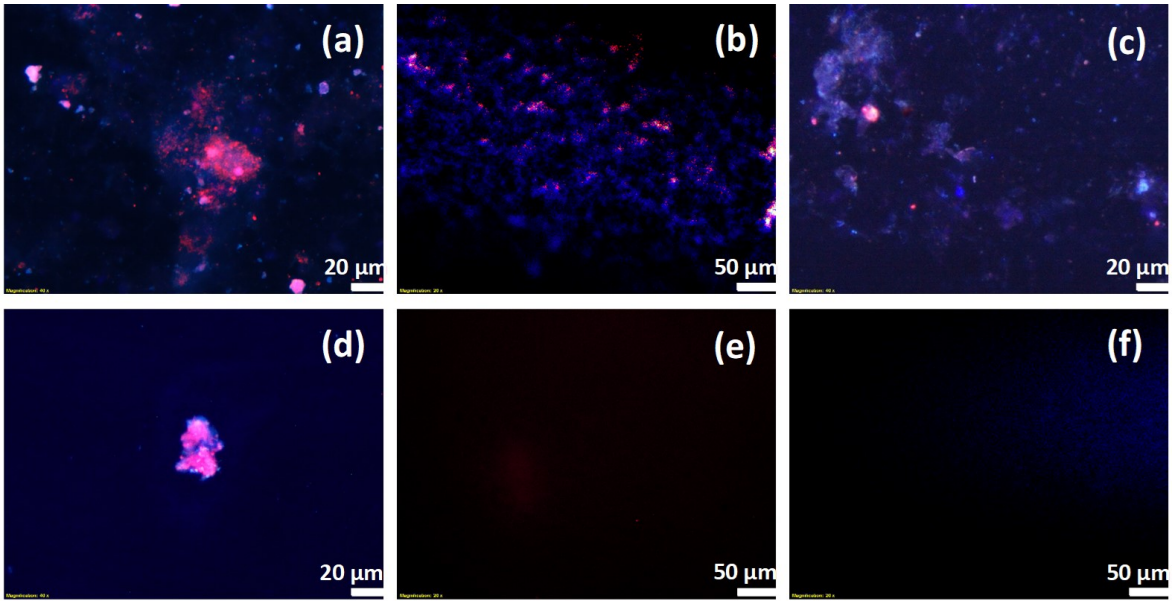

Figure 2. Optical microscope images of (a–d) fouled membranes showing both blue and red fluorescence, and (e and f) virgin membrane showing neither red (CTC) or blue (DAPI) fluorescence.

As highlighted in Figure 2, fouled membranes showed the presence of both DNA (blue stain from DAPI) and as well as actively respiring bacteria (red stain from CTC). Higher intensity of red fluorescence obfuscated the blue fluorescence in some regions of the membrane, for example, Figure 2(a),(d), shows the typical clustering of live bacteria. In contrast, blue fluorescence was more spread out indicating the existence of biofilms covering the membrane surface. Besides, the virgin membrane showed no fluorescence, Figure 2(e),(f), serving as a control and confirming the buildup of bacteria and biofilm in the form of fouling during filtration. To completely reproduce the experimental set-up, the numerical simulations were carried out without ammonium nitrogen, $S_1 = 0$ in the general mathematical model formulation, and the model was run by fixing a negligible initial autotrophic biofilm fraction $X_1 = 0.001$. In such specific situation, only heterotrophic bacteria can constitute the biofouling layer as their growth and evolution only require organic carbon S_2 and dissolved oxygen S_3.

A semi-continuous pressure sensor was used for transmembrane pressure measurement for the col-

lection of experimental data sets. These were constituted by more than 10,000 sampling points automatically collected with a time interval of around $0.001s$. The first data set, i.e., forward filtration for 20 *min*, was used to calibrate the model. Based on the characteristics of the fed wastewater, the concentration of dissolved compounds in the bulk liquid, such as ammonia S_1, organic carbon S_2, and oxygen S_3, was fixed at 0, 25, and 8 mgL^{-1}, respectively. Of course, the selection of these values was due to all standard procedures adopted for the preparation of the synthetic wastewater at a laboratory scale. The initial biofilm thickness was set to 50 μm, as it was assumed that a thin cake layer immediately appears on the membrane surface due to the presence of suspended bacteria and particles in the wastewater. The initial biofilm composition was characterized by a predominant heterotrophic bacteria component, whose activity is stimulated by the presence of organic carbon S_2 and dissolved oxygen S_3 under non-limiting conditions. The adopted initial autotrophic bacteria f_2 and inert materials f_3 volume fractions were 0.001 and 0.002%, respectively. The EPS volume fraction f_4, which usually depends on biofilm maturation and polymers production within the matrix during biofilm growth, was initially set to 0.05%. The biofilm component growth rates and kinetic constants were derived from previous studies [7, 35, 38]. Table 1 resumes all the kinetic constants and parameters adopted for numerical simulations.

Table 1. Kinetic parameters used for model simulations.

Parameter	Definition	Unit	Value	Reference
$K_{max,1}$	Maximum growth rate for X_1	d^{-1}	4.8	[7]
$K_{max,2}$	Maximum growth rate for X_2	d^{-1}	0.95	[7]
k_1	EPS formation by X_1	$mgCOD/mgCOD$	0.45	[44]
k_2	EPS formation by X_2	$mgCOD/mgCOD$	0.34	[44]
$K_{1,2}$	Organics half saturation constant for X_1	$mgCODl^{-1}$	5	[7]
$K_{1,3}$	Oxygen half saturation constant for X_1	mgl^{-1}	0.1	[7]
$K_{2,1}$	Ammonium half saturation constant for X_2	$mgNl^{-1}$	1	[7]
$K_{2,3}$	Oxygen half saturation constant for X_2	mgl^{-1}	0.1	[7]
b_1	Endogenous rate for X_1	d^{-1}	0.025	[7]
b_2	Endogenous rate for X_2	d^{-1}	0.0625	[7]
F_1	Biodegradable fraction of X_1	$--$	0.8	[7]
F_2	Biodegradable fraction of X_2	$--$	0.8	[7]
c_1	Decay-inactivation rate for X_1	d^{-1}	0.05	[7]
c_2	Decay-inactivation rate for X_2	d^{-1}	0.05	[7]
Y_1	Yield of X_1	$g_{biomass}/g_{substrate}$	0.4	[7]
Y_2	Yield of X_2	$g_{biomass}/g_{substrate}$	0.22	[7]
μ	Absolute viscosity of water	Nsm^{-1}	10^{-3}	[30]
ρ	Biofilm components density	gm^{-3}	2500	[7]
λ	Biomass shear constant	$m^{-1}d^{-1}$	1250	[7]
K	Sloughing constant	m^{-1}	55.5	This study

The model was able to reproduce the biofouling formation over time during forward and backwashing operations of the system. The biofilm growth rate was higher during forward filtration as the availability of substrates for the microbial species was higher than in the backwashing step. Indeed, the convection and diffusion of substrates within the biofilm was strongly influenced by the water flow direction and boundary conditions, as it is shown in Figure 3:

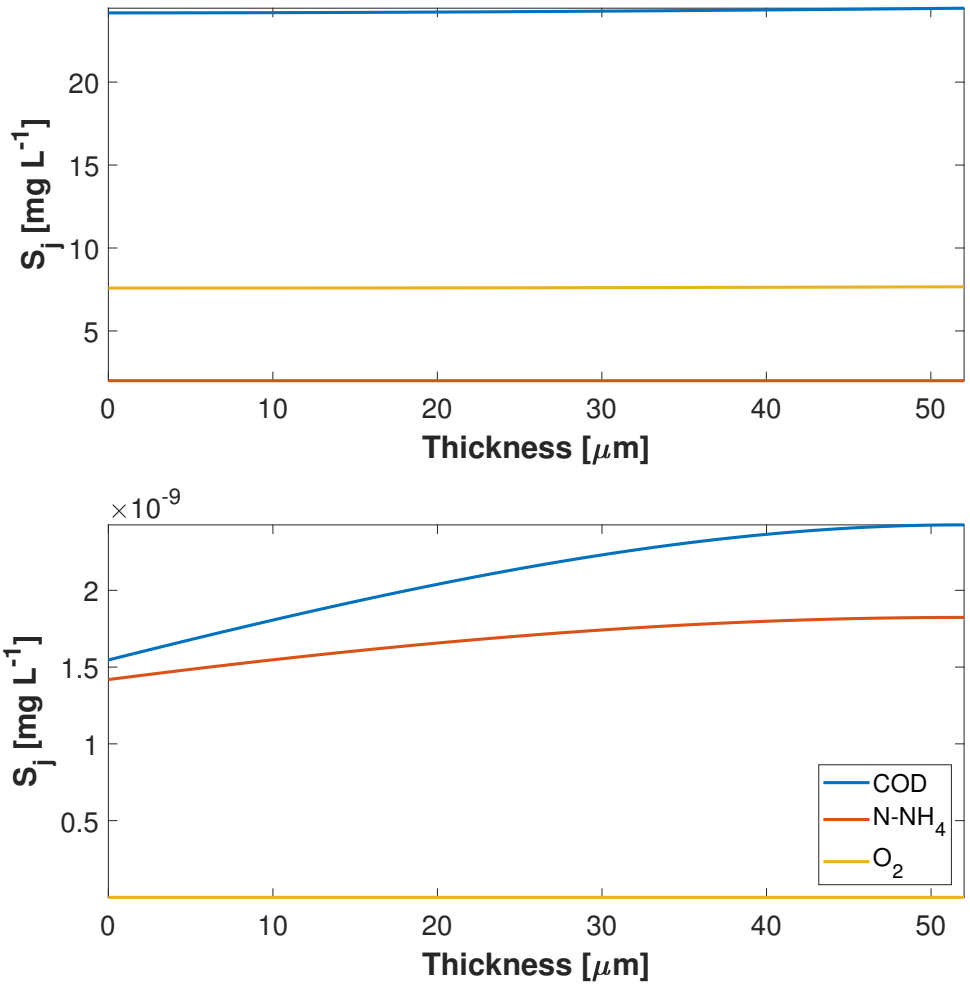

Figure 3. Substrate profiles during forward filtration (top) and backwashing operations (bottom). Note the y-axis scaling to low values.

During forward filtration, the biofilm profile results fully penetrated by dissolved substrates, which lead to higher kinetic growth rates than during the other operating conditions with relatively high COD concentration in the permeate water (Figure 3(top)). Conversely, pure water crosses the biofilm from the membrane surface to the boundary layer during backwashing, and the dissolved substrates are completely washed out from the biofilm layer. Figure 3(down) shows the extremely low substrate concentrations at the end of the backwashing phase.

For the newly introduced parameters, such as the hydraulic resistance of the membrane R_M, the specific resistance terms of each biofilm component $\alpha_i, i = 1, ..., n$, and the permanent biofouling layer L_{lim}, the values were obtained by comparing the model output and the experimental pressure drop data over time. The procedure will be explained in the next subsection. Table 2 resumes the adopted values for the initial condition of biofilm components and for substrate concentrations.

Table 2. Initial conditions for biofilm growth.

Parameter	Symbol	Unit	Value
Ammonia concentration at $L = L(t)$	S_{1L}	mgl^{-1}	0
Organic Carbon concentration at $L = L(t)$	S_{2L}	mgl^{-1}	25
Dissolved Oxygen concentration at $L = L(t)$	S_{3L}	mgl^{-1}	8
Initial Biofilm thickness	L_0	mm	0.05
Initial Volume Fraction of Heterotrophs (X_1)	$f_{1,0}(z)$	–	0.947
Initial Volume Fraction of Autotrophs (X_2)	$f_{2,0}(z)$	–	0.001
Initial Volume Fraction of Inert (X_3)	$f_{3,0}(z)$	–	0.002
Initial Volume Fraction of EPS (X_4)	$f_{4,0}(z)$	–	0.05

6. Calibration and validation

The hydraulic resistance of the membrane filter R_M and the specific hydraulic resistance values of each biofilm component $\alpha_i, i = 1, ..., n$ were obtained from the calibration procedure. The inclusion of R_M in the calibration protocol was due to the highly different values reported in the literature for similar microfiltration systems. The biological components, such as autotrophic X_1 and heterotrophic X_2 bacteria, were assumed to react in the same way to the hydraulic filtration stress. Therefore, their specific hydraulic resistance α_1 and α_2 were constrained to have the same value, i.e., $\alpha_1 = \alpha_2$. Similarly, the specific hydraulic resistance of the biologically produced components, such as inert material X_3 and EPS X_4, were constrained to have the same value, i.e., $\alpha_3 = \alpha_4$. Moreover, different permanent fouling layers L_{lim} were tested during the calibration. This parameter was added to the calibration procedure as Eq (2.5) has been newly introduced in the present work to account for backwashing procedures occurring in wastewater systems. Indeed, the detachment rate σ_d assumes an important rule in modeling of biofilm growth, as it usually dominates the dynamics of biofilm components for long-term behavior of the multispecies biological system [39]. In addition, the detachment occurring during backwashing procedures also affects the short-term filtration performance containing the pressure drop during forward filtration [45]. Experimental evidences demonstrated the presence of a permanent fouling layer which cannot be removed by traditional backwashing procedures using clean water [46]. In same cases, the use of specific chemical cleaning protocols represent the only solution to restore the membrane, and completely eradicate the permanent biofouling layer. Moreover, aggressive cleaning procedures can seriously damage the filtration membrane, shortening its operating life [46]. In the present case, a simple water cleaning procedures was adopted and a permanent fouling layer L_{lim} in the range of 0.01 and 0.05 mm was tested with numerical experiments.

The Matlab tool *fmincon* was used to find the best set of parameters $(R_M, \alpha_i, i = 1, ..., 4)$ and minimize the Euclidean norm (EN) between model prediction and experimental data. Equation (6.1) reports the discrete formulation of the minimized function used for the ΔP-based calibration:

$$EN = \sum_{k=1}^{\bar{k}} \sqrt{\left[J_k \mu \left(R_M + \rho \frac{L_k^2}{2L_0} \sum_{i=1}^{4} \alpha_{0,i} \, f_{i,k} \right) \right]^2 - \Delta \bar{P}_k{}^2}, \quad k = 1, ..., \bar{k}, \tag{6.1}$$

where the subscript k represents a specific measurement/sampling time, $\Delta \bar{P}_k$ is the observed experimental value at the specific sampling time, and $\bar{k}$ is the total number of samples. The procedure was

repeated for each permanent biofouling layer L_{lim} value, i.e., 0.01, 0.02, 0.03, 0.04, and 0.05, and the mean absolute relative error $\bar{\epsilon}$, Eq (6.2), was used to compare model predictions with experimental data:

$$\bar{\epsilon} = \frac{1}{\bar{k}} \sum_{k=1}^{\bar{k}} \left| \frac{\Delta P_{m,k} - \Delta \bar{P}_k}{\Delta \bar{P}_k} \right| 100, \quad k = 1, ..., \bar{k}, \tag{6.2}$$

where $\Delta P_{m,k}$ represent the model prediction at a specific sampling time. Note that the term $\Delta P_{m,k}$ in Eq (6.2) corresponds to $J_k \mu \left(R_M + \rho \frac{L_k^2}{2L_0} \sum_{i=1}^{4} \alpha_{0,i} \, f_{i,k} \right)$ in Eq (6.1).

The numerical analysis revealed a better fitting with experimental data when using higher values of L_{lim}. The higher was the permanent biofouling layer value, the lower mean absolute relative error $\bar{\epsilon}$ was observed, Figure 4.

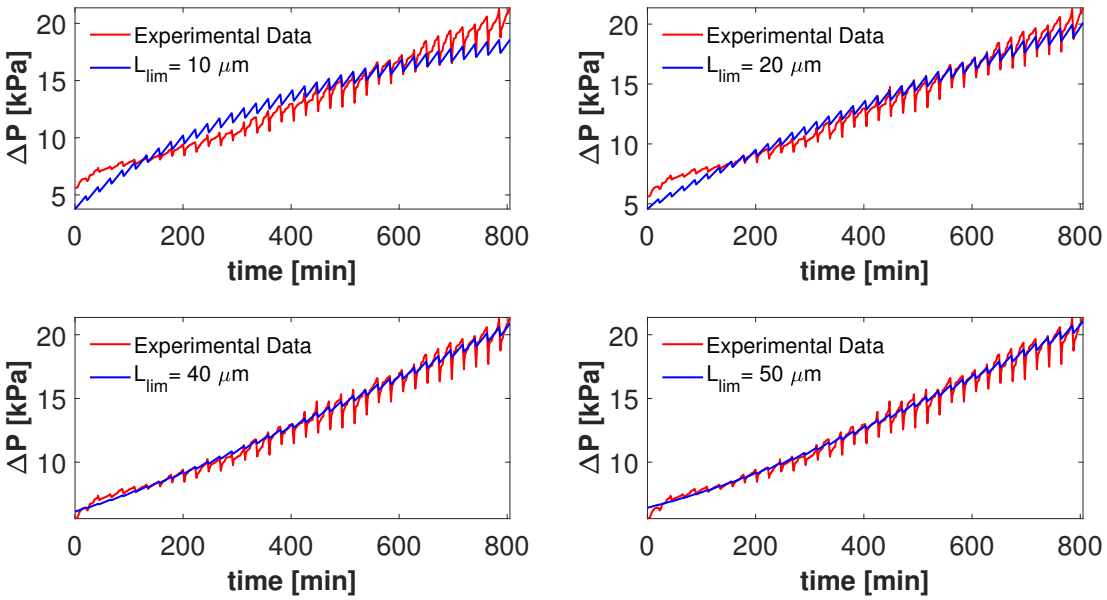

Figure 4. Numerical simulation with different permanent biofouling layer of 0.01, 0.02, 0.04, and 0.05 *mm*. The observed values of the mean absolute relative errors are 8.56, 4.98, 2.15, and 1.99%, respectively.

This result was due to the strong influence of the permanent biofouling layer on the detachment rate σ_d, Eq (2.5): when a low value of L_{lim} is applied, numerical simulations showed a lower accuracy compared with higher values. In particular, the model was not able to fit the increasing pressure drop occurring during the first part of the data set. Different values of L_{lim} led to different biofilm thickness profile over time. Figure 5 shows that the selection of the permanent fouling layer value is crucial to obtain a meaningful response from numerical simulations. Experimental evidences demonstrated a significant accumulation of biofilm on the top of the membrane, which cannot be reproduced using low biofouling layer values ($L_{lim} = 10 \, \mu m$ and $L_{lim} = 20 \, \mu m$).

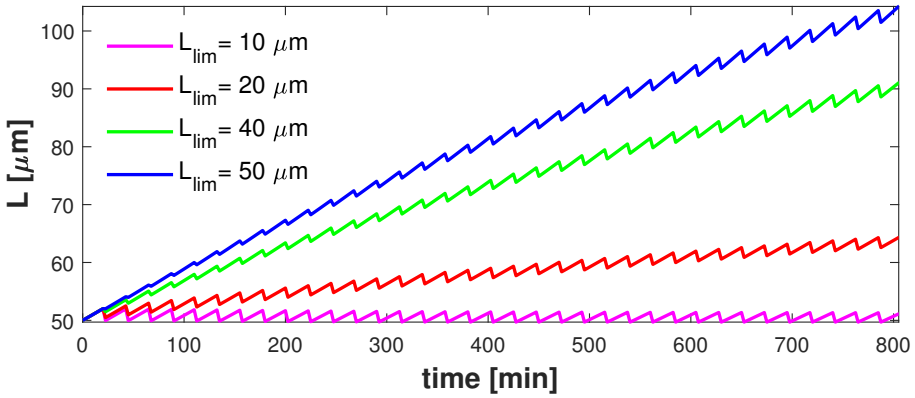

Figure 5. Biofilm thickness evolution using different L_{lim} values of 0.01, 0.02, 0.04, and 0.05 *mm*.

The best fit with experimental data $L_{lim} = 50\ \mu m$ was used for model calibration using the 20 *min* filtration dataset. The mean absolute relative error $\bar{\epsilon} = 1.99\%$ was achieved and the calibrated values ($R_M, \alpha_i, i = 1, ..., 4$, and L_{lim}) were used for model validation. Indeed, using the 40 *min* filtration dataset the model showed a mean absolute relative error $\bar{\epsilon} = 7.07\%$ as reported in Figure 6. For $L_{lim} > 50\ \mu m$ higher mean absolute relative error values were observed.

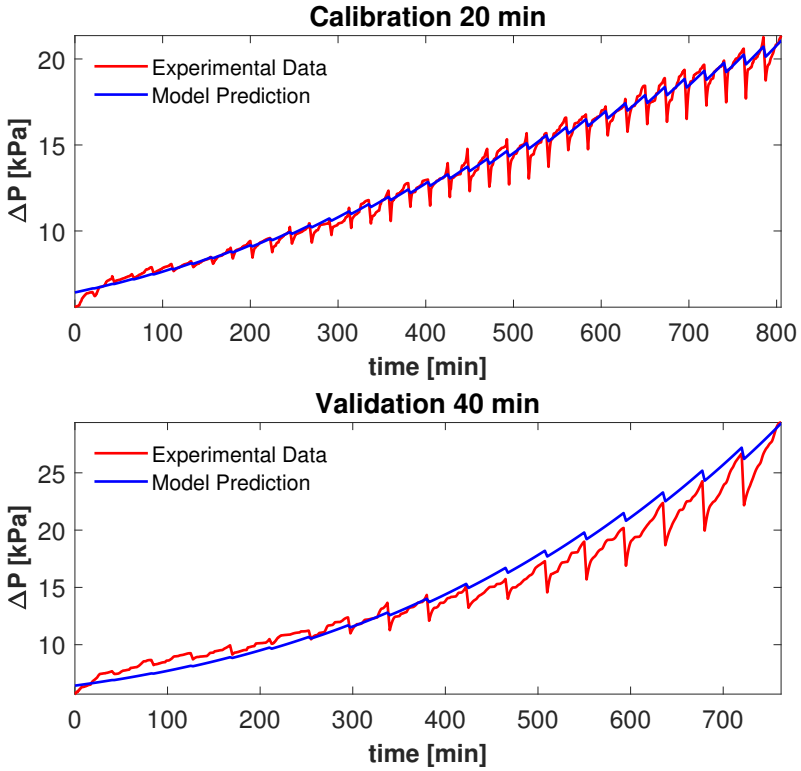

Figure 6. Model calibration with 20 *min* forward filtration (top, $\bar{\epsilon} = 1.99\%$) and model validation with 40 *min* forward filtration (bottom, $\bar{\epsilon} = 7.07\%$).

The calibrated parameters are summarized in Table 3.

Table 3. Calibrated parameters.

Parameter	Symbol	Unit	Value
Resistance of the clean membrane	R_M	mm^{-1}	$3.29 \cdot 10^5$
Specific resistance of heterotrophic bacteria (X_1)	α_1	$mmKg^{-1}$	$2.20 \cdot 10^5$
Specific resistance of autotrophic bacteria (X_2)	α_2	$mmKg^{-1}$	$2.20 \cdot 10^5$
Specific resistance of inert materials (X_3)	α_3	$mmKg^{-1}$	$1.34 \cdot 10^7$
Specific resistance of EPS (X_4)	α_4	$mmKg^{-1}$	$1.34 \cdot 10^7$
Permanent biofouling layer	L_{lim}	mm	0.05

Noteworthy, the specific hydraulic resistance related to the biologically produced components is one order magnitude higher than the bacterial species resistance. This is in accordance with the experimental evidence demonstrating that the hydraulic resistance of the whole biofouling layer can be attributed to the EPS formation during biofilm growth [21, 47].

The model was able to fit experimental data and predict with good accuracy the pressure drop occurring in the last part of the experiments. It can be noticed that the model underestimates the real pressure drop occurring from $t = 0$ to $t = 350$ *min*, while an opposite trend was observed during the last part of the experiment. The latter observation is crucial as the higher is the pressure levels needed in the membrane-biofilm system, the higher are operation costs occurring in real scale applications. This observation confers more relevance to higher pressure levels occurring during biofilm maturation, $t > 350$ *min*, than to the lower pressure drop characterizing the beginning of the experiment.

7. Conclusions

The presented mathematical model represents a direct connection between the conventional modeling of membrane filtration and the mathematical modeling of multispecies biofilm growth and dynamics. A novel formulation of the detachment rate has been introduced. It is able to account for the effect of backwashing/regeneration procedures on biofilm development. The crucial role micro-biologically produced compounds, such as EPS, accumulating in the biofouling layer during microfiltration processes has been addressed. The free-boundary problem of biofilm growth on a filtration support has been numerically solved using the method of characteristics. The model was calibrated and validated by using lab-scale experimental data of microfiltration. It was able to predict in a reasonable way the increase of transmembrane pressure during constant flux microfiltration. Future studies are still required to address specific biofilm and membrane behaviors occurring in larger scale applications for wastewater treatment. Numerical simulations confirmed the crucial role of the biofilm EPS matrix on membrane pressure drop. A next step might be the application of the model to different hydraulic regimes and different biological cases occurring in engineering water filtration systems.

Acknowledgments

Authors would like to acknowledge the project “Employing circular economy approach for OFMSW management within the Mediterranean countries - CEOMED” number A B.4.2 0058, funded

under the ENI CBC MED 2014-2020 programme and the project "METAGRO - bioMETanazione dei sottoprodotti della filiera AGROindustriale campana" CUP: B18H19005240009. The authors also acknowledges the support from: CARIPLO Foundation (progetto VOLAC, Grant number: 2017-0977). S. Chellam gratefully acknowledges funding from the National Science Foundation (CBET 1636104) and (CBET 2211035). N. Cogan acknowledges funding from the National Science Foundation (CBET 2210992).

This paper has been performed under the auspices of the GNFM of INdAM.

Conflict of interest

The authors declare there is no conflict of interest.

References

1. R. V. Linares, A. Wexler, S. S. Bucs, C. Dreszer, A. Zwijnenburg, H. C. Flemming, et al., Compaction and relaxation of biofilms, *Desalin. Water Treat.*, **57** (2016), 12902–12914. https://doi.org/10.1080/19443994.2015.1057036
2. K. Martin, D. Bolster, N. Derlon, E. Morgenroth, R. Nerenberg, Effect of fouling layer spatial distribution on permeate flux: a theoretical and experimental study, *J. Membr. Sci.*, **471** (2014), 130–137. https://doi.org/10.1016/j.memsci.2014.07.045
3. A. Venezuela, J. Pérez-Guerrero, S. Fontes, Hybrid modeling of convective laminar flow in a permeable tube associated with the cross-flow process, *Commun. Nonlinear Sci. Numer. Simul.*, **14** (2009), 795–810. https://doi.org/10.1016/j.cnsns.2007.11.009
4. S. F. Anis, R. Hashaikeh, N. Hilal, Microfiltration membrane processes: a review of research trends over the past decade, *J. Water Process Eng.*, **32** (2019), 100941. https://doi.org/10.1016/j.jwpe.2019.100941
5. I. Ivanovic, T. Leiknes, The biofilm membrane bioreactor (bf-mbr)—a review, *Desalin. Water Treat.*, **37** (2012), 288–295. https://doi.org/10.1080/19443994.2012.661283
6. B. D'Acunto, L. Frunzo, V. Luongo, M. R. Mattei, Invasion moving boundary problem for a biofilm reactor model, *Eur. J. Appl. Math.*, **29** (2018), 1079–1109. https://doi.org/10.1017/S0956792518000165
7. B. D'Acunto, L. Frunzo, V. Luongo, M. R. Mattei, Modeling heavy metal sorption and interaction in a multispecies biofilm, *Mathematics*, **7** (2019), 781. https://doi.org/10.3390/math7090781
8. A. Trucchia, M. Mattei, V. Luongo, L. Frunzo, M. Rochoux, Surrogate-based uncertainty and sensitivity analysis for bacterial invasion in multi-species biofilm modeling, *Commun. Nonlinear Sci. Numer. Simul.*, **73** (2019), 403–424. https://doi.org/10.1016/j.cnsns.2019.02.024
9. C. Dreszer, J. S. Vrouwenvelder, A. H. Paulitsch-Fuchs, A. Zwijnenburg, J. C. Kruithof, H. C. Flemming, Hydraulic resistance of biofilms, *J. Membr. Sci.*, **429** (2013), 436–447. https://doi.org/10.1016/j.memsci.2012.11.030
10. S. Kang, W. Lee, S. Chae, H. Shin, Positive roles of biofilm during the operation of membrane bioreactor for water reuse, *Desalination*, **202** (2007), 129–134. https://doi.org/10.1016/j.desal.2005.12.048

11. S. Kerdi, A. Qamar, A. Alpatova, N. Ghaffour, An in-situ technique for the direct structural characterization of biofouling in membrane filtration, *J. Membr. Sci.*, **583** (2019), 81–92. https://doi.org/10.1016/j.memsci.2019.04.051
12. W. Bowen, J. Calvo, A. Hernandez, Steps of membrane blocking in flux decline during protein microfiltration, *J. Membr. Sci.*, **101** (1995), 153–165. https://doi.org/https://doi.org/10.1016/0376-7388(94)00295-A
13. S. Chellam, W. Xu, Blocking laws analysis of dead-end constant flux microfiltration of compressible cakes, *J. Colloid Interface Sci.*, **301** (2006), 248–257. https://doi.org/10.1016/j.jcis.2006.04.064
14. N. Cogan, S. Chellam, Incorporating pore blocking, cake filtration, and eps production in a model for constant pressure bacterial fouling during dead-end microfiltration, *J. Membr. Sci.*, **345** (2009), 81–89. https://doi.org/10.1016/j.memsci.2009.08.027
15. M. Imran, H. L. Smith, A model of optimal dosing of antibiotic treatment in biofilm, *Math. Biosci. Eng.*, **11** (2014), 547. https://doi.org/10.3934/mbe.2014.11.547
16. C. Laspidou, L. Spyrou, N. Aravas, B. Rittmann, Material modeling of biofilm mechanical properties, *Math. Biosci.*, **251** (2014), 11–15. https://doi.org/10.1016/j.mbs.2014.02.007
17. M. Mattei, L. Frunzo, B. D'Acunto, Y. Pechaud, F. Pirozzi, G. Esposito, Continuum and discrete approach in modeling biofilm development and structure: a review, *J. Math. Biol.*, **76** (2018), 945–1003. https://doi.org/10.1007/s00285-017-1165-y
18. A. Tenore, M. Mattei, L. Frunzo, Modelling the ecology of phototrophic-heterotrophic biofilms, *Commun. Nonlinear Sci. Numer. Simul.*, **94** (2021), 105577. https://doi.org/10.1016/j.cnsns.2020.105577
19. A. Tenore, F. Russo, M. Mattei, B. D'Acunto, G. Collins, L. Frunzo, Multiscale modelling of de novo anaerobic granulation, *Bull. Math. Biol.*, **83** (2021), 1–50. https://doi.org/10.1007/s11538-021-00951-y
20. M. Jafari, N. Derlon, P. Desmond, M. C. van Loosdrecht, E. Morgenroth, C. Picioreanu, Biofilm compressibility in ultrafiltration: a relation between biofilm morphology, mechanics and hydraulic resistance, *Water Res.*, **157** (2019), 335–345. https://doi.org/10.1016/j.watres.2019.03.073
21. H. Vrouwenvelder, C. Dreszer, R. V. Linares, J. Kruithof, C. Mayer, H. Flemming, Why and how biofilms cause biofouling–the "hair-in-sink"-effect, in *The Perfect Slime: Microbial Extracellular Polymeric Substances (EPS)*, (2016), 193–206.
22. G. Tierra, J. P. Pavissich, R. Nerenberg, Z. Xu, M. S. Alber, Multicomponent model of deformation and detachment of a biofilm under fluid flow, *J. R. Soc. Interface*, **12** (2015), 20150045. https://doi.org/10.1098/rsif.2015.0045
23. M. Li, K. Matouš, R. Nerenberg, Predicting biofilm deformation with a viscoelastic phase-field model: modeling and experimental studies, *Biotechnol. Bioeng.*, **117** (2020), 3486–3498. https://doi.org/10.1002/bit.27491
24. M. Rahimi, S. Madaeni, M. Abolhasani, A. A. Alsairafi, Cfd and experimental studies of fouling of a microfiltration membrane, *Chem. Eng. Process. Process Intensif.*, **48** (2009), 1405–1413. https://doi.org/10.1016/j.cep.2009.07.008

25. A. Tenore, J. Vieira, L. Frunzo, V. Luongo, M. Fabbricino, Calibration and validation of an activated sludge model for membrane bioreactor wastewater treatment plants, *Environ. Technol.*, **41** (2020), 1923–1936. https://doi.org/10.1080/09593330.2018.1551940

26. M. Zare, F. Z. Ashtiani, A. Fouladitajar, Cfd modeling and simulation of concentration polarization in microfiltration of oil–water emulsions; application of an eulerian multiphase model, *Desalination*, **324** (2013), 37–47. https://doi.org/10.1016/j.desal.2013.05.022

27. C. Picioreanu, J. Vrouwenvelder, M. Van Loosdrecht, Three-dimensional modeling of biofouling and fluid dynamics in feed spacer channels of membrane devices, *J. Membr. Sci.*, **345** (2009), 340–354. https://doi.org/10.1016/j.memsci.2009.09.024

28. J. Shin, K. Kim, J. Kim, S. Lee, Development of a numerical model for cake layer formation on a membrane, *Desalination*, **309** (2013), 213–221. https://doi.org/10.1016/j.desal.2012.10.018

29. S. Chellam, N. Cogan, Colloidal and bacterial fouling during constant flux microfiltration: comparison of classical blocking laws with a unified model combining pore blocking and eps secretion, *J. Membr. Sci.*, **382** (2011), 148–157. https://doi.org/10.1016/j.memsci.2011.08.001

30. N. Cogan, J. Li, A. R. Badireddy, S. Chellam, Optimal backwashing in dead-end bacterial microfiltration with irreversible attachment mediated by extracellular polymeric substances production, *J. Membr. Sci.*, **520** (2016), 337–344. https://doi.org/10.1016/j.memsci.2016.08.001

31. B. D'Acunto, L. Frunzo, V. Luongo, M. Mattei, A. Tenore, Free boundary problem for the role of planktonic cells in biofilm formation and development, *Z. Angew. Math. Phys.*, **72** (2021), 1–17. https://doi.org/10.1007/s00033-021-01561-3

32. Y. Rohanizadegan, S. Sonner, H. J. Eberl, Discrete attachment to a cellulolytic biofilm modeled by an itô stochastic differential equation, *Math. Biosci. Eng.*, **17** (2020), 2236–2271. https://doi.org/10.3934/mbe.2020119

33. F. Russo, A. Tenore, M. R. Mattei, L. Frunzo, Multiscale modelling of the start-up process of anammox-based granular reactors, *Math. Biosci. Eng.*, **19** (2022), 10374–10406. https://doi.org/10.3934/mbe.2022486

34. O. Wanner, W. Gujer, A multispecies biofilm model, *Biotechnol. Bioeng.*, **28** (1986), 314–328. https://doi.org/10.1002/bit.260280304

35. B. D'Acunto, L. Frunzo, M. Mattei, On a free boundary problem for biosorption in biofilms, *Nonlinear Anal. Real World Appl.*, **39** (2018), 120–141. https://doi.org/10.1016/j.nonrwa.2017.06.010

36. B. D'Acunto, L. Frunzo, I. Klapper, M. Mattei, Modeling multispecies biofilms including new bacterial species invasion, *Math. Biosci.*, **259** (2015), 20–26. https://doi.org/10.1016/j.mbs.2014.10.009

37. J. M. Hughes, H. J. Eberl, S. Sonner, A mathematical model of discrete attachment to a cellulolytic biofilm using random des, *Math. Biosci. Eng.*, **19** (2022), 6582–6619, https://doi.org/10.3934/mbe.2022310

38. C. S. Laspidou, B. E. Rittmann, Non-steady state modeling of extracellular polymeric substances, soluble microbial products, and active and inert biomass, *Water Res.*, **36** (2002), 1983–1992. https://doi.org/10.1016/S0043-1354(01)00414-6

39. F. Abbas, R. Sudarsan, H. J. Eberl, Longtime behavior of one-dimensional biofilm models with shear dependent detachment rates, *Math. Biosci. Eng.*, **9** (2012), 215–239. https://doi.org/10.3934/mbe.2012.9.215

40. E. Morgenroth, P. A. Wilderer, Controlled biomass removal—the key parameter to achieve enhanced biological phosphorus removal in biofilm systems, *Water Sci. Technol.*, **39** (1999), 33–40. https://doi.org/10.1016/S0273-1223(99)00147-X

41. D. Dubber, N. F. Gray, Replacement of chemical oxygen demand (cod) with total organic carbon (toc) for monitoring wastewater treatment performance to minimize disposal of toxic analytical waste, *J. Environ. Sci. Health A*, **45** (2010), 1595–1600. https://doi.org/10.1080/10934529.2010.506116

42. I. Douterelo, J. B. Boxall, P. Deines, R. Sekar, K. E. Fish, C. A. Biggs, Methodological approaches for studying the microbial ecology of drinking water distribution systems, *Water Res.*, **65** (2014), 134–156. https://doi.org/10.1016/j.watres.2014.07.008

43. M. E. Sieracki, T. L. Cucci, J. Nicinski, Flow cytometric analysis of 5-cyano-2, 3-ditolyl tetrazolium chloride activity of marine bacterioplankton in dilution cultures, *Appl. Environ. Microbiol.*, **65** (1999), 2409–2417. https://doi.org/10.1128/AEM.65.6.2409-2417.1999

44. B. Merkey, B. Rittmann, D. Chopp, Modeling how soluble microbial products (SMP) support heterotrophic bacteria in autotroph-based biofilms, *J. Theor. Biol.*, **259** (2009), 670–683. https://doi.org/10.1016/j.jtbi.2009.05.010

45. W. Guo, H. H. Ngo, J. Li, A mini-review on membrane fouling, *Bioresour. Technol.*, **122** (2012), 27–34. https://doi.org/10.1016/j.biortech.2012.04.089

46. J. Mansouri, S. Harrisson, V. Chen, Strategies for controlling biofouling in membrane filtration systems: challenges and opportunities, *J. Mater. Chem.*, **20** (2010), 4567–4586. https://doi.org/10.1039/B926440J

47. N. Cogan, S. Chellam, A method for determining the optimal back-washing frequency and duration for dead-end microfiltration, *J. Membr. Sci.*, **469** (2014), 410–417. https://doi.org/10.1016/j.memsci.2014.06.052

Appendix

Other model modifications

The newly introduced formulation for the biofilm hydraulic resistance, $R_B(t)$ in Eqs (2.1) and (2.8), was obtained by comparing the real available experimental data with different theoretical formulations of the pressure drop occurring during MBR operations. Linear (Eq (A.1)) and quadratic (Eqs (A.2)–(A.4)) correlations between the pressure drop ΔP and the biofilm thickness were derived from mass balance principles, and the following formulations

$$\Delta P(t) = J\mu\left(R_m + \sum_{i=1}^{n} \alpha_{0,i} \int_0^{L(t)} f_i \rho_i dz\right), \tag{A.1}$$

$$\Delta P(t) = J\mu\left(R_m + \sum_{i=1}^{n} \alpha_{0,i} \int_0^{L(t)} \frac{2 f_i \rho_i}{L_0} z dz\right), \tag{A.2}$$

$$\Delta P(t) = J\mu\left(R_m + \sum_{i=1}^{n} \alpha_{0,i} \int_0^{L(t)} \frac{f_i \rho_i}{L_0} z dz\right), \tag{A.3}$$

$$\Delta P(t) = J\mu\left(R_m + \sum_{i=1}^{n} \alpha_{0,i} \int_0^{L(t)} f_i \rho_i \left(1 + \frac{z}{L_0}\right) dz\right). \tag{A.4}$$

were tested using the same minimizing tool *fmincon* to compare model predictions and lab scale data in all the performed numerical experiments. This means that the different formulations presented in Eqs (A.1)–(A.4) were used during the calibration and validation steps and when changing the model initial conditions. An typical result is shown in Figure A.1, where the minimum mean average errors, were obtained by using Eqs (A.2) and (A.3). Indeed, these formulations are quite similar as they differently consider the effect of the hydraulic resistance of biological and non-biological components by scaling the values of the parameters $\alpha_{0,i}, i = 1, ..., 4$ by a factor of 2. The Eq (A.3) was then used for the general model formulation, as in some cases the mean average relative error was lower than the observed value obtained by using Eq (A.2).

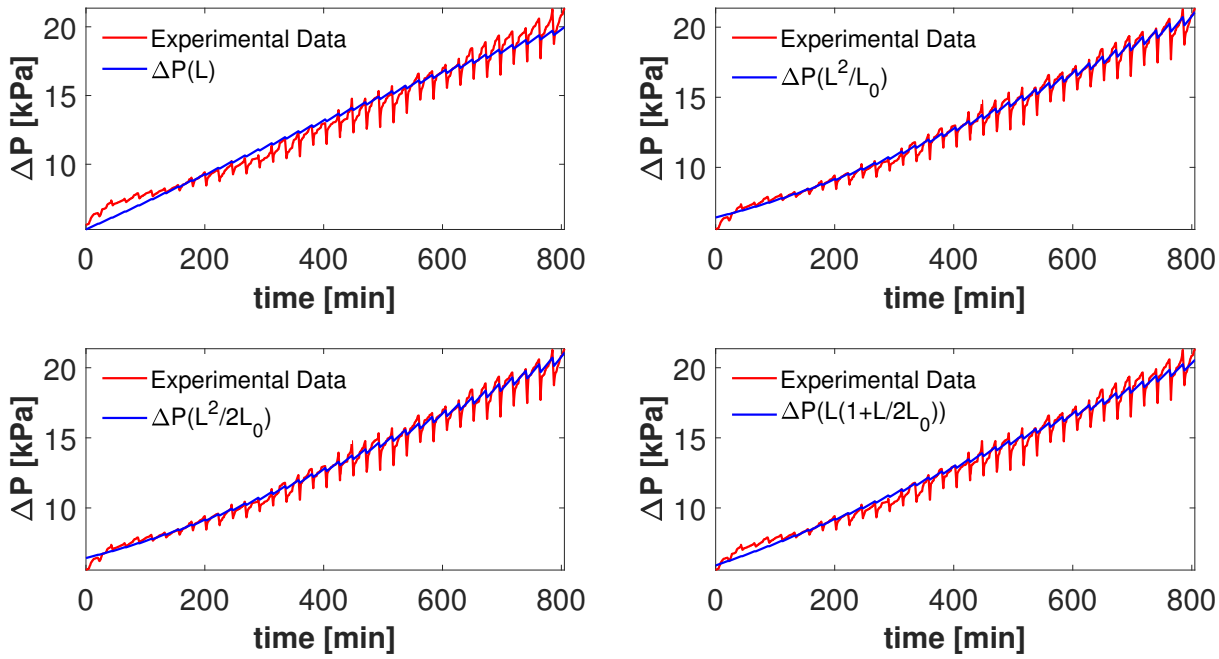

Figure A.1. Numerical simulation with different $\Delta P(t)$ formulations. The relative errors obtained using Eqs (A.1)–(A.4), are 4.22, 1.99, 1.99, and 2.67%, respectively.

A quadratic correlation of the pressure drop ΔP and the biofilm thickness allows for a more reasonable data fitting, and Eqs (A.2) and (A.3) showed the best results. Indeed, Eqs (A.1)–(A.4) were individually used to determine the pressure drop in all the numerical experiments performed during the calibration and validation phases. For instance, the mean average relative error trend related to each simulation set with increasing L_{lim} was also analyzed to test the accuracy of the matematical model in fitting the pressure drop experimental data. Figure A.2 shows the trends of the error occurring when

increasing the permanent biofouling layer from 0.01 to 0.05 *mm*. The 20 *min* and 40 *min* data-sets were used as example.

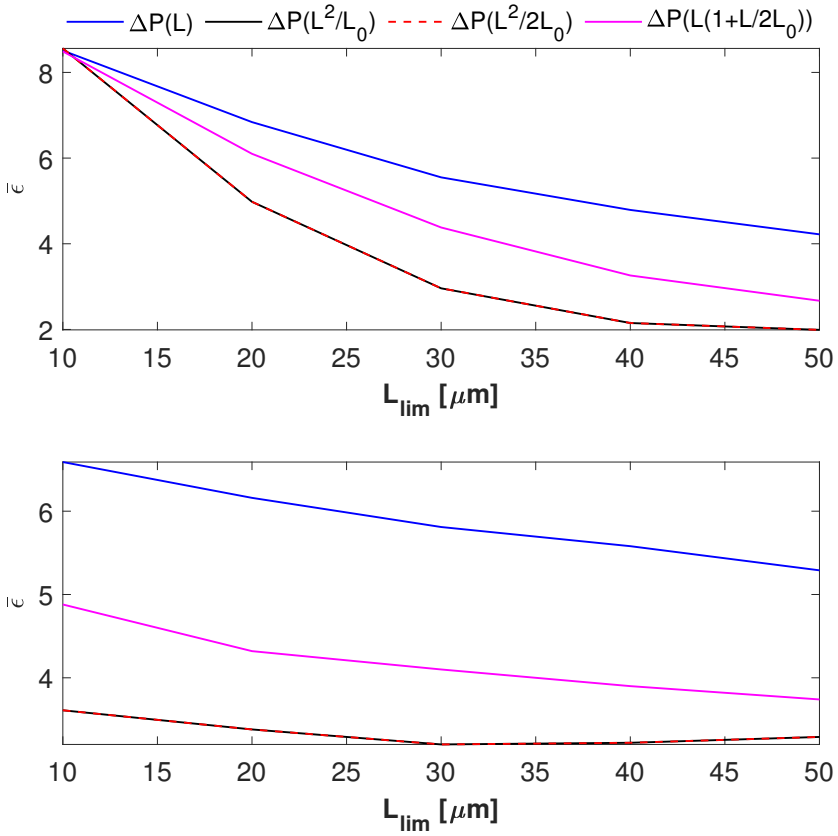

Figure A.2. Mean average relative error trends with different $\Delta P(t)$ formulations obtained with 20 *min* (top), and 40 *min* (bottom) forward filtration.

It can be noticed that with 20 *min* forward filtration the error shows a fast decreasing trend when increasing the permanent biofouling layer, exactly as the second order norm calculated for the optimization. When 40 *min* forward filtration data are used, the minimum mean average error is higher then the one obtained in the first case, and it shows a slight increase when increasing the L_{lim} value, Figure A.2. This behavior can be attributed to the more difficult prediction of the effective pressure drop and biofilm thickness when increasing the filtration time. In this case, the effect of the sloughing is more impulsive and the model results are less accurate than in the case of limited forward filtration time. Further experiment are still required to describe the error trends when higher values of L_{lim} are used for the detachment rate.

The effect of the erosion term λL^2 in the newly introduced detachment Eq (2.5) was also investigated. Numerical simulations were run with fixing $\lambda = 0$ instead of $\lambda = 1250\ mmd^{-1}$. It is well known that the erosion term has a significant effect in long-term simulations as it regulates the maximum biofilm thickness representing a negative rate in the free boundary Eq (2.4) [39]. In the present case, the limited forward filtration time does not allow the erosion term to significantly affect biofilm growth and evolution. To generalize the problem, the term λL^2 was not removed from Eq (2.5). This

can be useful to test the model on different engineering systems where longer forward filtration phases are adopted. In the present work, the results showed a similar trend of the relative errors in all the tested cases and confirmed the negligible influence of the erosion term on the detachment rate (data not shown).

Finally, other numerical simulations were performed by decreasing the initial volume fraction of the EPS component within the biofilm (from 0.05 to 0.01%). The obtained results (data not shown) showed a very similar trend of the pressure drop profile, but a better fit with experimental data was obtained when using an EPS volume fraction of 0.05 (data not shown). This evidence could be ascribed to the presence of EPS in the wastewater. These compounds immediately contribute to increase the pressure drop during the initial phase of microfiltration. Indeed, the result confirms the negligible effect of the EPS matrix on the pressure drop during the initial phase of the experiment, and the highly relevant effect of the same component during biofilm growth and maturation.

AIMS Press